2016

First Measurement of Horizontal Wind and Temperature in the Lower Thermosphere (105–140 km) with a Na Lidar at Andes Lidar Observatory

Alan Liu
Embry-Riddle Aeronautical University, liuz2@erau.edu

Yafang Guo

Fabia A. Vargas
Department of Electrical and Computer Sciences, University of Illinois at Urbana-Champaign

Gary Swenson,
University of Illinois at Urbana-Champaign

Scholarly Commons Citation

Liu, A. Z., Y. Guo, F. Vargas, and G. R. Swenson (2016), First measurement of horizontal wind and temperature in the lower thermosphere (105–140 km) with a Na Lidar at Andes Lidar Observatory, Geophys. Res. Lett., 43, doi:10.1002/2016GL068461

AGU PUBLICATIONS

Geophysical Research Letters

RESEARCH LETTER
10.1002/2016GL068461

Key Points:
- Na Lidar at ALO measured neutral wind and temperature up to 140 km when thermospheric Na was present, covering 60 km altitude range
- Lidar winds are consistent with rocket measurements and show diurnal to semidiurnal tide transition from mesopause to the thermosphere
- Larger power aperture lidars have the potential to provide routine measurement of the neutral atmosphere in the entire *D* and *E* regions

Correspondence to:
A. Z. Liu,
alan.liu@erau.edu

Citation:
Liu, A. Z., Y. Guo, F. Vargas, and G. R. Swenson (2016), First measurement of horizontal wind and temperature in the lower thermosphere (105–140 km) with a Na Lidar at Andes Lidar Observatory, *Geophys. Res. Lett.*, *43*, doi:10.1002/2016GL068461.

Received 27 FEB 2016
Accepted 1 MAR 2016
Accepted article online 6 MAR 2016

First measurement of horizontal wind and temperature in the lower thermosphere (105–140 km) with a Na Lidar at Andes Lidar Observatory

Alan Z. Liu[1,2], Yafang Guo[1], Fabio Vargas[2], and Gary R. Swenson[2]

[1]Center for Space and Atmospheric Research, Department of Physical Sciences, Embry-Riddle Aeronautical University, Daytona Beach, Florida, USA, [2]Department of Electrical and Computer Engineering, University of Illinois at Urbana-Champaign, Urbana, Illinois, USA

Abstract We report the first measurement of nighttime atmospheric temperature and horizontal wind profiles in the lower thermosphere up to 140 km with the Na lidar at Andes Lidar Observatory in Cerro Pachón, Chile (30.25°S, 70.74°W), when enhanced thermospheric Na was observed. Temperature and horizontal wind were derived up to 140 km using various resolutions, with the lowest resolution of about 2.7 hr and 15 km above 130 km. Thus, the measurements span 60 km in vertical, more than double the traditional 25 km. On the night of 17 April 2015, the horizontal wind magnitude in the thermosphere exceeds 150 ms^{-1}, consistent with past rocket measurements. The meridional wind shows a clear transition from the diurnal-tide-dominant mesopause to the semidiurnal-tide-dominant lower thermosphere. A lidar with a 100 times the power aperture product will be able to measure wind and temperature above 160 km and cover longer time span, providing key measurements for the study of atmosphere-space interactions in this region.

1. Introduction

It is well known that neutral wind in the thermosphere is extremely important for the electrodynamics in both *E* and *F* regions of the ionosphere. The neutral-ion interactions drive a complex electric field that are responsible for many variabilities in the ionosphere. Studies have also shown that the atmospheric disturbances from below, such as gravity waves [e.g., *Fritts et al.*, 2009], planetary waves [*Liu et al.*, 2010], and tides [*Immel et al.*, 2006; *Hagan et al.*, 2007] are responsible for a variety of phenomena in the ionosphere, including equatorial spread *F*, plasma bubbles, and longitudinal variations of electron density. Gravity waves also have strong impact on the mean state of the thermosphere even in the *F* region [*Yigit et al.*, 2012]. Successful modeling of the ionosphere-thermosphere systems [*Richmond et al.*, 1992; *Fesen et al.*, 2000] crucially depends on accurate knowledge of the neutral wind in this region [*Huba et al.*, 2010]. However, measurement of the neutral wind in the thermosphere has long been a challenge, especially at high vertical and temporal resolutions necessary to resolve the atmospheric disturbances. In the mesopause and lower thermosphere extended (MLT-X) region (80–200 km), the only accurate, high vertical resolution wind measurements are obtained through rocket experiments with chemical releases and resonance-florescence Doppler lidars. Empirical models such as the horizontal wind model (HWM) [*Drob et al.*, 2008] provide the mean global wind field but does not include short periods and spatial scale disturbances necessary to study thermosphere variabilities. *Larsen and Fesen* [2009] compared rocket measurements of over 500 wind profiles since late 1950s with the HWM and showed that the model agrees reasonably well with the average wind but significantly underestimates the maximum wind and shear.

Narrow-band resonance-fluorescence lidars have long been used for measuring the fundamental atmospheric quantities including temperature and wind in the mesopause region (80–105 km). The technique is based on detecting the thermal broadening and Doppler shift of atomic spectral lines of the mesospheric metals, mainly Na [*Gardner*, 2004], which is relatively abundant and has large effective backscattering cross section for resonance-fluorescence scattering. The Na layer exists mainly in the 80–105 km altitude range due to meteoric ablation [*Plane*, 2003], which dictates the range of lidar measurements. When enough Na

is present, the Na lidar measurement of wind is highly accurate, as demonstrated by comparisons with the advection velocities from meteor trails [*Grime et al.*, 2000] and the rocket measurement [*Larsen et al.*, 2003], both conducted at Starfire Optical Range, New Mexico, and with colocated meteor radar wind measurement at Maui [*Franke et al.*, 2005].

In recent years, several lidar sites around the world reported observations of metal layers in the lower thermosphere [*Gerding et al.*, 2001; *Gong et al.*, 2003; *Höffner and Friedman*, 2004, 2005; *Chu et al.*, 2011; *Friedman et al.*, 2013; *Xue et al.*, 2013; *Gao et al.*, 2015], reaching as high as 155 km [*Chu et al.*, 2011] for Fe and up to 170 km [*Gao et al.*, 2015] for Na. While most of these observations were made with broadband lidars that cannot measure Doppler wind, the existence of these high-altitude metal layers raises the potential possibility of using narrow-band metal lidars to extend the temperature and wind measurement into the lower thermosphere. Since there is no other instrument currently capable of measuring nighttime neutral temperature and wind in this region, this potential capability is a significant advancement in upper atmosphere remote sensing. The continuous coverage of the neutral atmosphere in both time (over several hours at night) and altitude (80–140 km or higher) provides information on the short-period variabilities and their evolution from the upper mesosphere across the turbopause into the lower thermosphere. This will provide crucial information in this poorly known region, where many important coupling processes between the neutral atmosphere and ionosphere occur and where the behaviors of many disturbances change quickly as they propagate from a well-mixed homosphere into the molecular-diffusion-dominated heterosphere.

In this study we present the first observations of thermospheric Na with a narrow-band Na wind/temperature lidar. The lidar is located at Andes Lidar Observatory (ALO) in Cerro Pachón, Chile (30.25°S, 70.74°W). Recently, the thermospheric Na was observed on many nights over several months since May 2014. While the observation of thermospheric Na layer is of great scientific interest, it will be analyzed in detail in a separate study. In this work, our focus is on the lidar capability of measuring thermospheric horizontal wind and temperature. We will show that with the presence of thermospheric Na, temperature and horizontal wind measurement can be extended into the lower thermosphere up to 140 km with the current system. Furthermore, we show that a more powerful lidar will likely be able to extend such measurement to even higher altitude (above 150 km) and cover the entire *E* region with the presence of small amount of Na. In the next section, the recent Na lidar campaigns at ALO are described, followed by brief description of the features of the measured thermospheric Na. In section 3, we describe the method used to derive temperature and wind in the thermosphere and provide estimates of their uncertainties. Comparisons are made with the MSIS [*Hedin*, 1991; *Picone et al.*, 2002] and HWM [*Drob et al.*, 2008]. The results are summarized in section 4 with discussion on the capability of future more powerful lidars in extending measurement further into the thermosphere region.

2. ALO Lidar and Thermospheric Na Layer

The ALO Na lidar was upgraded in May 2014 with a high-power amplified diode laser (TA-SHG Pro from Toptica Photonis, Inc.) as the master oscillator, replacing an aging Coherent Ring Dye Laser. The receiver optics was also improved with more efficient optical coupling from the telescope to the PMT as described in *Smith and Chu* [2015]. These combined improvements resulted in nearly uninterrupted nightly lidar operations in several following campaigns, with signals of over 1000 counts per laser pulse from the Na layer at about 0.4–0.6 Wm^2 power aperture product. Four campaigns were conducted after the upgrade, in August–September 2014, January–February 2015, April 2015, and July 2015. The ALO lidar measures the Na density, line-of-sight wind, and temperature profiles in zenith (*Z*), and 20° off-zenith to east (E) and south (S). Before January 2015, the lidar was operated in zenith direction only. Starting in January 2015, the lidar was operated in ZSE sequence, with 60 or 90 s integration time at each direction on most nights. Horizontal winds are measured when the lidar was operated in this mode. Table 1 lists the number of total observation nights after the upgrade and the number of nights when thermospheric Na were observed. Out of 58 nights, the thermospheric Na were observed on 13 nights, and they appeared during the May 2014, August–September 2014 and April 2015 campaigns, with a total of 32 nights. There was no thermospheric Na observed in any of the 21 nights in January-February 2015 and July 2015 campaigns. Therefore this thermospheric Na is not a persistent feature, and their appearance has large month-to-month variations. In the months that they do appear, their occurrence rate is quite high, average at about 40%.

An example of the observed thermospheric Na on the night of 17 April 2015 is shown in Figure 1. The contour is plotted using the raw calculated Na density, at vertical resolution of 500 m, and temporal resolution of 60 s.

Table 1. Numbers of Nights of Lidar Observations in Five Campaigns Since May 2014 Upgrade[a]

	May 2014	Aug–Sep 2014	Jan–Feb 2015	Apr 2015	July 2015	Total
Total nights	3 (2)	16 (5)	16 (0)	13 (6)	10 (0)	58 (13)
Horizontal wind mode	0	0	6 (0)	8 (5)	10 (0)	24 (5)

[a]The numbers of nights when thermospheric Na were observed are in the parentheses. The numbers of nights when horizontal wind were measured are listed in the second row.

No smoothing or interpolation was used. Note that a nonlinear color scale is used to highlight the low density of thermospheric Na. On this night, the Na appeared at about 160 km after 3 UT, gradually moving downward, and reaching 120 km at about 6UT. The Na density in the thermosphere varies from 1–2 cm^{-3} to 5 cm^{-3}. Note it is possible that Na also exists in the white region with lower density (< 1 cm^{-3}) but is too low to be detected. This pattern is common on almost all nights when the thermospheric Na was present, with some variations in appearance time and descending rate.

3. Thermospheric Wind and Temperature

The presence of thermospheric Na makes it possible to derive temperature and horizontal wind in this region. The nights when both horizontal wind were measured and the thermospheric Na were present are during the April 2015 campaign, on 17–19, 21, and 23. Data from these nights are used to extend the horizontal wind and temperature measurements into the lower thermosphere. The results on 17 are presented here. The results from other nights are similar with some differences in the range of derived wind and temperature due to different Na densities and lidar signal levels.

The Na lidar at ALO measures the wind and temperature using the three-frequency technique [*She and Yu*, 1994]. The laser is locked at the Na resonance frequency at the D2a line, and the two frequencies shifted by ±630 MHz in a sequence. The temperature and line-of-sight wind are derived based on the ratios among the backscattered signals at these three frequencies [*Krueger et al.*, 2015, and references therein]. The wind and temperature errors with the three-frequency technique are dominated by the photon noise, which follows the Poisson distribution. For the Na lidar system, the rms temperature and line-of-sight wind errors, as described in equations (8) and (26) in *Gardner* [2004], are mainly determined by the signal-to-noise ratio (SNR),

$$\mathrm{SNR} = \frac{N}{\sqrt{N+B}}, \tag{1}$$

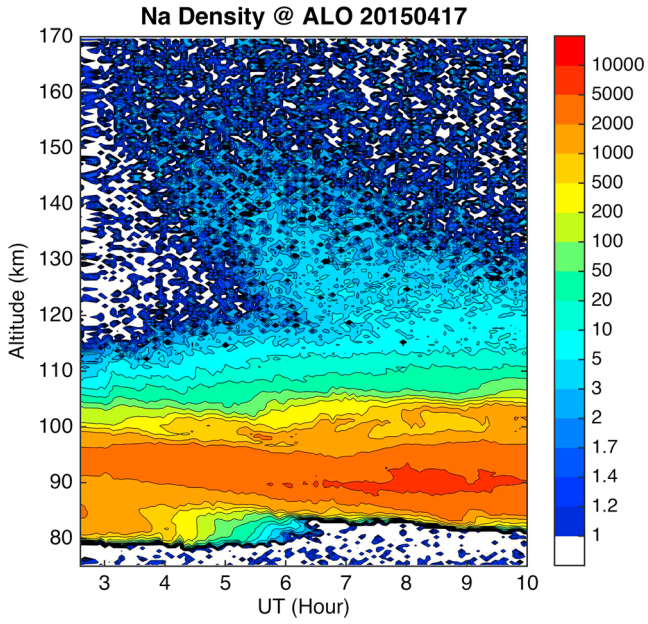

Figure 1. Na density (atoms per cm^3) on the night of 17 April 2015 measured by the Na lidar at Andes Lidar Observatory in Cerro Pachón, Chile. Nonlinear color scale is used to highlight the low density in the thermosphere.

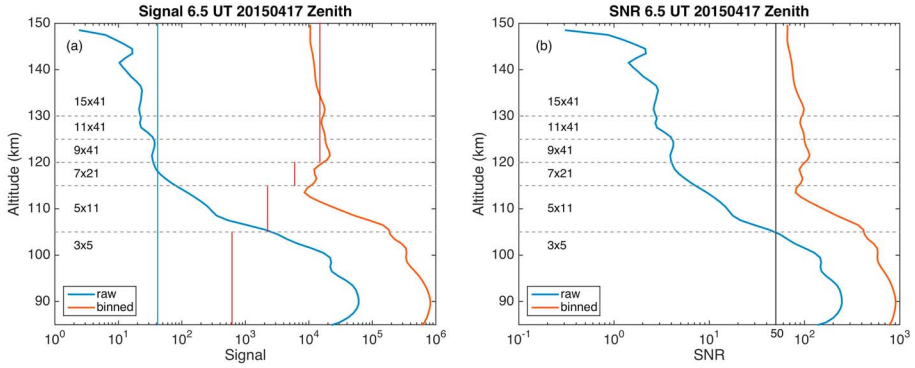

Figure 2. (a) Signal and (b) SNR profiles at 6.5 UT on 17 April 2015 when the lidar was pointed at zenith, smoothed with a 5 km full width Hamming window. The raw profile (blue) is at 1 min, 1 km resolutions. The binned profile (red) is obtained by binning photon counts with an n km bin in vertical and by adding up m consecutive profiles, centered at the altitude and time in question. Different values of n and m are used in different altitude ranges as indicated by the dashed horizontal lines and the numbers on the left as $n \times m$.

where N is the Na signal and B is the background photon count. Note that this definition of SNR is equivalent to the square root of the SNR defined in *Gardner* [2004].

As seen in Figure 1, the Na density in the thermosphere, though detectable, is 3–4 orders of magnitude smaller than at the peak of the Na layer. To examine the signal distribution in more detail, we show in Figure 2 the signal and SNR profiles at 6.5 UT on this night when the lidar was pointed at zenith. These profiles are smoothed with a 5 km full width Hamming window to remove small scale fluctuations. The blue lines in Figures 2a and 2b are from raw photon counts at 1 km, 1 min resolutions. They show that above 117 km, the background becomes larger than the signal and the SNR drops below 5. To increase the SNR at high altitudes, while still maintain higher resolutions at lower altitudes, we divided the altitude range into several regions at 105 km, 115 km, 120 km, 125 km, and 130 km, as marked by horizontal dashed lines in Figure 2. In each region, the signals are binned in vertical with an n km window and in time by adding m consecutive profiles, all centered at the altitude and time in question. The specific values of n and m are indicated in Figure 2 in all layers. The signal, background, and SNR after binning are shown as red lines. Even though the binning does not change the relative magnitude between the background and the signal, the SNR is increased by a factor of $\sqrt{n \times m}$. After binning, the SNR is above 50 at all altitudes up to 150 km. This is about the same as the SNR at 100 km before binning, so we can expect that reasonable temperature and wind can be derived.

During the night, the lidar was pointed to zenith, and 20° off-zenith to south and east in sequence, with 60 s integration time at each direction. With additional time for laser beam steering, it takes 80 s to complete one profile. The profiles in the east was used to derive the zonal wind; the profiles in the south were used to derive the meridional wind as well as the temperature, because the meridional signal is the highest. The binning

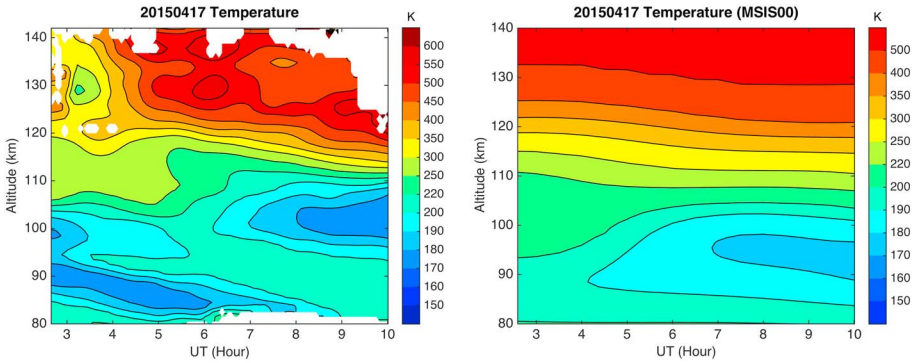

Figure 3. Temperature on 17 April 2015 (left) and corresponding MSIS temperature (right) on the same night. Note the nonlinear contour intervals used to accommodate the rapid temperature increase in the thermosphere.

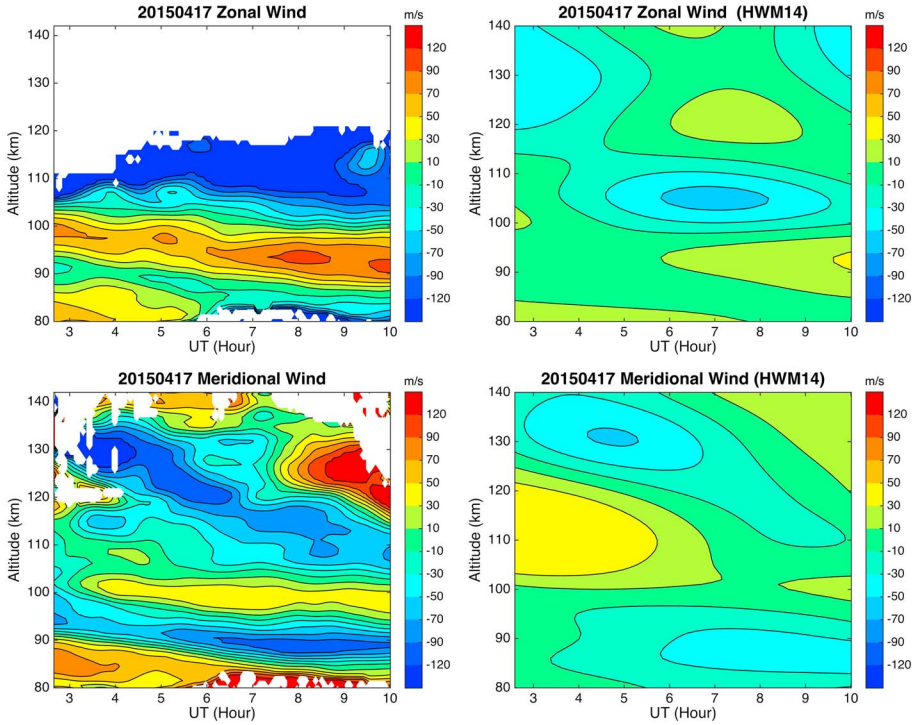

Figure 4. Zonal (top) and meridional (bottom) winds on 17 April 2015 (left) and corresponding HWM14 winds (right) on the same night.

was done separately in each direction. Therefore, the total time span of binning m profiles in one direction is $80\text{s} \times m \times 3 = 4m$ min. Therefore, binnings of 5, 11, 21, and 41 profiles in different layers correspond to time spans of 20, 44, 84, and 164 min, respectively.

The derived temperature and horizontal wind using the binned profiles are shown in Figures 3 and 4, respectively. The white regions are where the signals are too low to derive temperature and wind. The contours are smoothed with 5 km and a 1 h full width Hamming windows. The derived temperature from south can reach 135 km throughout most of the night and sometimes can reach 140 km. It shows a rapid increase from below 300 K to above 400 K in a narrow layer less than 5 km, which descends from above 120 km around 4 UT to 110 km at 10 UT. The similar feature is also visible in the MSIS contour. Higher in the thermosphere above 125 km, the measured temperature exceeds 500 K. The MSIS temperature also increases to above 500 K, but the increase is slower than the lidar measurement.

The zonal wind shown in Figure 4a only reaches 120 km, because the lidar signal is smaller in this direction. There is strong westward wind between 105 and 120 km throughout the night. In Figure 4c, the measured meridional wind reached can reach up to 140 km. There is a clear downward progression of the maximum southward wind from about 130 km at 4 UT to 110 km at 9 UT. Below 105 km, there is downward progression of alternating southward/northward winds at slower rate. It is clear that the structures are associated with the diurnal tide below 105 km and with the semidiurnal tide above. Because of the large vertical range coverage of over 50 km, the transition from the mesopause where the diurnal tide is dominant to the lower thermosphere where the semidiurnal tide is dominant is clearly measured by the lidar.

Comparing with the HWM wind in Figures 4b and 4d, we can identify some similarities, such as the westward wind between 100 and 100 km, and the transition from diurnal tide to semidiurnal tide in the meridional wind. Overall, the HWM winds are much smaller than the lidar measurement. This is expected because the HWM only represents the mean wind field. The magnitude of the lidar measured horizontal wind is around 150 to 200 ms^{-1}, comparable with decades of sounding rocket measurements [*Larsen*, 2002] and Incoherent Scatter Radar measurements [*Fesen et al.*, 1993; *Larsen and Fesen*, 2009].

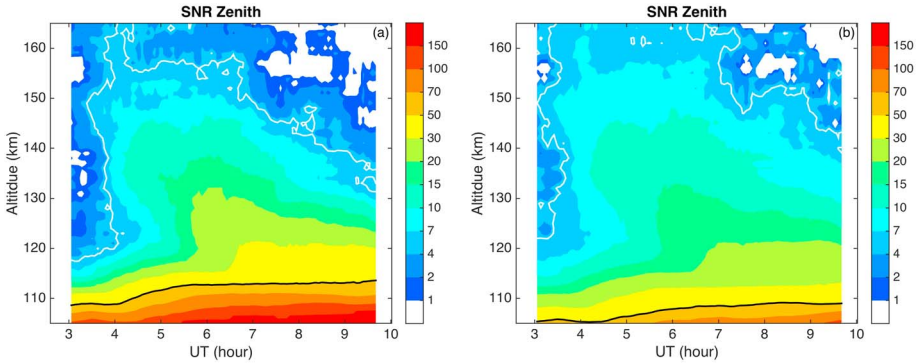

Figure 5. Signal-to-noise ratios in zenith direction on 17 April 2015, binned with 5 km vertical bin size and summed over 11 profiles. The white and black lines indicate SNR = 5 and 50, respectively. The white region is where SNR < 1. (a) Calculated with measured signal and background. (b) Calculated with no background noise and the signal reduced by a factor of 5, simulating the effect of a daytime filter.

4. Conclusions

We have demonstrated that the ALO Na lidar with a modest 0.4–0.6 Wm^2 power aperture product is capable of measuring the nighttime neutral atmosphere temperature and wind measurement well into the lower thermosphere up to 140 km, when the thermospheric Na is present. This has significantly increased the altitude range of Na lidar measurements from the traditional 25 km (80–105 km) to 60 km, covering almost the entire *E* region. One of the scientific values of such measurement is illustrated in the meridional wind, which shows the simultaneous measurement of the diurnal tides in the mesopause region and the semidiurnal tide in the thermosphere.

The thermospheric Na and other metals were not observed by ground-based lidars until recent years, mainly due to improvement in lidar technology which significantly increased the signal. Recent lidar observations have shown that the thermospheric metals are not a rare phenomenon. Satellite observations [*Gardner et al.*, 1999] have also shown that there exists a permanent, low-density neutral Na up to 300 km, with maxima near dawn and dust and around the magnetic equator. This suggests that the thermospheric Na is not limited to the color area shown in Figure 1. A Na lidar with a larger power aperture product will be able to detect Na at lower density, therefore cover larger vertical range and longer time period. To illustrate this, we show in Figure 5a the SNR on 17 April 2015 in zenith direction with photon counts binned using $n = 5$ and $m = 11$, the same binning parameters used for the layer between 105 and 115 km. A black line highlights where SNR = 50, the value when reasonable temperature and wind can be derived. A white line marks where SNR = 5. If the power aperture product of the lidar is increased by a factor of 100, the SNR will increase by a factor of 10, so all the area below the white line will have SNR > 50, and wind and temperature can be derived at the resolution of 5 km and 21 profiles (corresponding to as short as 21 min, or 84 min in the current ALO lidar operation mode). If the resolution is further reduced by a factor of 5, wind and temperature in all the colored area can be derived. Since a major part of the photon noise in the lower thermosphere is from the background, the technique used in daytime lidar measurement, which involves using Faraday filters [*She*, 2004; *Krueger et al.*, 2015] to reduce the background, may also be used. Typically, such filters can reduce the background to negligible level but also reduces the signal. To exam the effectiveness of this, we neglected the background and reduced the signal by a factor of 5 to recalculate the SNR, which is shown in Figure 5b. It shows that the SNR is reduced at lower altitude but is increased above. Combining this with a much larger power aperture product lidar, it can be expected that wind and temperature measurements can be extended above 150 km. One such powerful lidar system is recently proposed in the report of the Observatory for Atmosphere Space Interactions (OASIS) [*Gardner et al.*, 2014]. It will be able to provide measurements of the neutral atmosphere in the mesosphere lower thermosphere-extended (MLT-X) region, providing key information for the study of both neutral and electrodynamics and the atmosphere-space interactions.

Acknowledgments

The ALO laser upgrade was made possible with the National Science Foundation (NSF) Major Research Instrument grant AGS-1229085 for the acquisition of the laser. The grant supported Wentao Huang and John Smith for their engineering work in the testing and installation of the laser and the improvement of the receiver system. The grant also supported the initial campaign and subsequent improvement of the lidar system. The Na lidar at ALO is part of the Consortium of Resonance and Rayleigh Lidars, supported by the Geospace Facilities program at NSF via grants AGS-1136278 and AGS-1136208. The ALO building construction was funded by the Department of Electrical and Computer Engineering, University of Illinois at Urbana-Champaign. We are grateful for the excellent support provided by the Cerro Pachón facility managed by the Association of Universities for Research in Astronomy.
Y. Guo's work is partially supported by NSF grants AGS-1110199 and AGS-1115249. The regular ALO Na Lidar data between 80 and 105 km, and contour plots are available at http://lidar.erau.edu/data/nalidar/. The processed thermospheric wind and temperature data are available upon request.

References

Chu, X., Z. Yu, C. S. Gardner, C. Chen, and W. Fong (2011), Lidar observations of neutral Fe layers and fast gravity waves in the thermosphere (110-155 km) at McMurdo (77.8°S, 166.7°E), Antarctica, *Geophys. Res. Lett.*, *38*, L23807, doi:10.1029/2011GL050016.

Drob, D. P., et al. (2008), An empirical model of the Earth's horizontal wind fields: HWM07, *J. Geophys. Res.*, *113*, A12304, doi:10.1029/2008JA013668.

Fesen, C. G., M. E. Hagan, C. A. Tepley, and R. G. Roble (1993), On the coupling between the lower and the upper thermosphere during the first lower thermosphere coupling study, *J. Geophys. Res.*, *98*(A2), 1545–1558.
Fesen, C. G., G. Crowley, R. G. Roble, A. D. Richmond, and B. G. Fejer (2000), Simulation of the pre-reversal enhancement in the low latitude vertical ion drifts, *Geophys. Res. Lett.*, *27*(13), 1851–1854.
Franke, S. J., X. Chu, A. Z. Liu, and W. K. Hocking (2005), Comparison of meteor radar and Na Doppler lidar measurements of winds in the mesopause region above Maui, Hawaii, *J. Geophys. Res.*, *110*, D09S02, doi:10.1029/2003JD004486.
Friedman, J. S., X. Chu, C. G. M. Brum, and X. Lu (2013), Observation of a thermospheric descending layer of neutral K over Arecibo, *J. Atmos. Sol. Terr. Phys.*, *104*(0), 253–259.
Fritts, D. C., et al. (2009), Overview and summary of the Spread *F* Experiment (SpreadFEx), *Ann. Geophys.*, *27*(5), 2141–2155.
Gao, Q., X. Chu, X. Xue, X. Dou, T. Chen, and J. Chen (2015), Lidar observations of thermospheric Na layers up to 170 km with a descending tidal phase at Lijiang (26.7°N, 100.0°E), China, *J. Geophys. Res. Space Physics*, *120*(10), 9213–9220.
Gardner, C. S. (2004), Performance capabilities of middle-atmosphere temperature lidars: comparison of Na, K, Ca, Ca^+, and Rayleigh systems, *Appl. Opt.*, *43*(25), 4941–4956.
Gardner, C. S., P. J. Espy, J. M. Forbes, D. L. Hysell, H.-L. Liu, J. M. C. Plane, M. Rapp, G. R. Swenson, and J. T. Thayer (2014), OASIS: Exploring the Interaction of Earth's Atmosphere with Space. An Atmospheric and Geospace Sciences Report Submitted to NSF. [Available at http://rsss.csl.illinois.edu/workshop.]
Gardner, J., A. Broadfoot, W. McNeil, S. Lai, and E. Murad (1999), Analysis and modeling of the GLO-1 observations of meteoric metals in the thermosphere, *J. Atmos. Sol. Terr. Phys.*, *61*(7), 545–562.
Gerding, M., M. Alpers, J. Höffner, and U. von Zahn (2001), Sporadic Ca and Ca+ layers at mid-latitudes: Simultaneous observations and implications for their formation, *Ann. Geophys.*, *19*(1), 47–58.
Gong, S. S., G. T. Yang, J. M. Wang, X. W. Cheng, F. Q. Li, and W. X. Wan (2003), A double sodium layer event observed over Wuhan, China by lidar, *Geophys. Res. Lett.*, *30*(5), 1209, doi:10.1029/2002GL016135.
Grime, B. W., T. J. Kane, A. Z. Liu, G. C. Papen, C. S. Gardner, M. C. Kelley, C. Kruschwitz, and J. Drummond (2000), Meteor trail advection observed during the 1998 Leonid shower, *Geophys. Res. Lett.*, *27*(13), 1819–1822.
Hagan, M. E., A. Maute, R. G. Roble, A. D. Richmond, T. J. Immel, and S. L. England (2007), Connections between deep tropical clouds and the Earth's ionosphere, *Geophys. Res. Lett.*, *34*, L20109, doi:10.1029/2007GL030142.
Hedin, A. E. (1991), Extension of the MSIS thermosphere model into the middle and lower atmosphere, *J. Geophys. Res.*, *96*(A2), 1159–1172.
Höffner, J., and J. S. Friedman (2004), The mesospheric metal layer topside: A possible connection to meteoroids, *Atmos. Chem. Phys.*, *4*, 801–808.
Höffner, J., and J. S. Friedman (2005), The mesospheric metal layer topside: Examples of simultaneous metal observations, *J. Atmos. Sol. Terr. Phys.*, *67*(13), 1226–1237.
Huba, J. D., G. Joyce, J. Krall, C. L. Siefring, and P. A. Bernhardt (2010), Self-consistent modeling of equatorial dawn density depletions with SAMI3, *Geophys. Res. Lett.*, *37*, L03104, doi:10.1029/2009GL041492.
Immel, T. J., E. Sagawa, S. L. England, S. B. Henderson, M. E. Hagan, S. B. Mende, H. U. Frey, C. M. Swenson, and L. J. Paxton (2006), Control of equatorial ionospheric morphology by atmospheric tides, *Geophys. Res. Lett.*, *33*, L15108, doi:10.1029/2006GL026161.
Krueger, D. A., C.-Y. She, and T. Yuan (2015), Retrieving mesopause temperature and line-of-sight wind from full-diurnal-cycle Na lidar observations, *Appl. Opt.*, *54*(32), 9469–9489.
Larsen, M. F. (2002), Winds and shears in the mesosphere and lower thermosphere: Results from four decades of chemical release wind measurements, *J. Geophys. Res.*, *107*(A8), 1215, doi:10.1029/2001JA000218.
Larsen, M. F., and C. G. Fesen (2009), Accuracy issues of the existing thermospheric wind models: Can we rely on them in seeking solutions to wind-driven problems?, *Ann. Geophys.*, *27*(6), 2277–2284, doi:10.5194/angeo-27-2277-2009.
Larsen, M. F., A. Z. Liu, R. L. Bishop, and J. H. Hecht (2003), Tomex: A comparison of lidar and sounding rocket chemical tracer wind measurement, *Geophys. Res. Lett.*, *30*(7), 1375, doi:10.1029/2002GL015678.
Liu, H.-L., W. Wang, A. D. Richmond, and R. G. Roble (2010), Ionospheric variability due to planetary waves and tides for solar minimum conditions, *J. Geophys. Res.*, *115*, A00G01, doi:10.1029/2009JA015188.
Picone, J. M., A. E. Hedin, D. P. Drob, and A. C. Aikin (2002), NRLMSISE-00 empirical model of the atmosphere: Statistical comparisons and scientific issues, *J. Geophys. Res.*, *107*(A12), 1468, doi:10.1029/2002JA009430.
Plane, J. M. C. (2003), Atmospheric chemistry of meteoric metals, *Chem. Rev.*, *103*(12), 4963–4984.
Richmond, A. D., E. C. Ridley, and R. G. Roble (1992), A thermosphere/ionosphere general circulation model with coupled electrodynamics, *Geophys. Res. Lett.*, *19*(6), 601–604.
She, C.-Y. (2004), Initial full-diurnal-cycle mesopause region lidar observations: Diurnal-means and tidal perturbations of temperature and winds over Fort Collins, CO (41°N,105°W), *J. Atmos. Sol. Terr. Phys.*, *66*(6–9), 663–674.
She, C. Y., and J. R. Yu (1994), Simultaneous three-frequncy Na lidar measurements of radial wind and temperature in the mesopause region, *Geophys. Res. Lett.*, *21*(17), 1771–1774.
Smith, J. A., and X. Chu (2015), High-efficiency receiver architecture for resonance-fluorescence and Doppler lidars, *Appl. Opt.*, *54*(11), 3173–3184.
Xue, X. H., X. K. Dou, J. Lei, J. S. Chen, Z. H. Ding, T. Li, Q. Gao, W. W. Tang, X. W. Cheng, and K. Wei (2013), Lower thermospheric-enhanced sodium layers observed at low latitude and possible formation: Case studies, *J. Geophys. Res. Space Physics*, *118*, 2409–2418, doi:10.1002/jgra.50200.
Yigit, E., A. S. Medvedev, A. D. Aylward, A. J. Ridley, M. J. Harris, M. B. Moldwin, and P. Hartogh (2012), Dynamical effects of internal gravity waves in the equinoctial thermosphere, *J. Atmos. Sol. Terr. Phys.*, *90–91*, 104–116.